Monolithic 160 Gbit/s optical time-division multiplexer

Jie Huang,* Carsten Langrock, X. P. Xie, and M. M. Fejer

Ginzton Laboratory, Stanford University, Stanford, California 94305, USA
**Corresponding author: jiehuang@stanford.edu*

Received May 17, 2007; accepted July 9, 2007;
posted July 18, 2007 (Doc. ID 83109); published August 6, 2007

We present the design and experimental characterization of a monolithic optical time-division multiplexer (MUX) for 160 Gbit/s operation based on periodically poled lithium niobate (PPLN) waveguides. Its key figures of merit agree well with theoretical predictions and meet or exceed those of a previously demonstrated PPLN–planar-light-wave-circuit hybrid MUX. The monolithic design has a simpler layout and higher efficiency while keeping the cross talk low. © 2007 Optical Society of America

OCIS codes: 190.4360, 070.4340, 230.1150, 190.2620.

Among several types of all-optical multiplexer (MUX) demonstrated for optical time-division multiplexing (OTDM) systems [1], the gated-mixer-based MUX has the advantage of providing stable operation with minimal fluctuation in pulse separations [2]. Previously 160 Gbit/s OTDM was demonstrated in periodically poled lithium niobate (PPLN) waveguides integrated with a planar-light-wave circuit [2,3]. In this Letter we report the design and experimental characterization of a monolithic MUX capable of 40 Gbit/s$\times$4 operation based entirely on a PPLN substrate. By tailoring and integrating multiple optical signal processing functions, we are able to use one instead of four PPLN waveguides and eliminate the use of additional couplers and silica-on-silicon circuitry, hence achieving a monolithic layout and higher efficiency.

The PPLN MUX is shown schematically in Fig. 1. A 40 GHz optical clock in the C band is injected into the device. The clock pulse is doubled to its second harmonic (SH) and filtered by the four-peak transfer function of a phase-modulated quasi-phase-matching (QPM) grating [4]. Observed in the time domain, the SH clock remains a 40 GHz pulse train, while, in the wavelength domain, each clock pulse now exhibits four discrete wavelength peaks. We can view the new SH clock as four perfectly synchronized 40 GHz clocks with four different colors; they become the four phases of a 160 GHz clock.

Next, the four-phase clock enters a section of four segmented sampling gratings, with length L_{sg} each and center-to-center separation L_u. The QPM period of each sampling grating is chosen such that its SH phase-matching wavelength equals the center wavelength of the corresponding clock phase. Four 40 Gbit/s data channels at different wavelengths are also coupled into the gratings.

In each sampling grating, the difference frequencies are generated between the phase-matched clock wavelength and each data channel. Altogether, 16 pulses are generated in the 4 gratings. Their frequencies form a matrix, where elements in the same column are generated in the same grating by one of the clock phases, and elements in the same row are from the same data channel. The frequencies of the data and clock pulses can be paired such that all diagonal elements are equal (Table 1). Using a bandpass filter at that common frequency, we are able to select just those four pulses.

The timing of the four pulses is the direct consequence of each pulse's being generated in a different sampling grating. Due to group-velocity mismatch between the C-band signal and the SH clock, the signal pulse generated in an earlier grating leads the next one by $\Delta t = \delta\nu L_u$. In a 160 Gbit/s system $\Delta t = 6.25$ ps. Given $\delta\nu = 0.36$ ps/mm in PPLN waveguides [5], we need $L_u = 17.36$ mm. Since $\delta\nu$ and L_u are both fixed, the timing is as accurate as the clock itself.

If the transfer functions of adjacent sampling gratings partly overlap, elements in the same row of Table 1 have common frequency components, which pass the bandpass filter and become interchannel cross talk at other time slots. To minimize cross talk, the sampling gratings are apodized to suppress the transfer function sidelobes, using the techniques developed in Ref. [6].

We now describe the theory to evaluate the MUX performance. The nonlinear optical process is cascaded SH generation (SHG) and difference frequency generation (DFG) in two separate gratings, with the SH of the external clock being the pump of the subsequent DFG in the sampling gratings. The carrier frequencies of the OTDM signal (ω_s), SH clock (ω_c), and data (ω_d) satisfy $\omega_s = \omega_c - \omega_d$. If the data bandwidth is sufficiently narrow compared with the pump bandwidth of each sampling grating, in the undepleted pump, unamplified signal, and lossless limit, for a given data channel the transfer function for the cascaded process is given by

$$\hat{A}_{os}(\Omega) = f(\Omega)\hat{D}_{sg}(\Omega)\hat{D}_{cg}(\Omega)\hat{A}_{cl}^2(\Omega)E_d, \qquad (1)$$

where E_d is the field amplitude of that data channel at frequency ω_d. Ω is the frequency detuning from ω_s

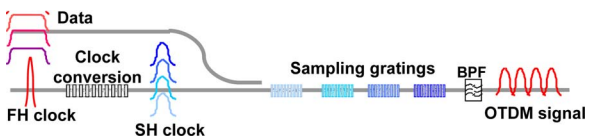

Fig. 1. (Color online) Schematic of the PPLN OTDM MUX.

Table 1. Generated Signal Frequencies (SGs)[a]

Channel	SG I	SG II	SG III	SG IV
1	$\omega_{p1}-\omega_{d1}$	$\omega_{p2}-\omega_{d1}$	$\omega_{p3}-\omega_{d1}$	$\omega_{p4}-\omega_{d1}$
2	$\omega_{p1}-\omega_{d2}$	$\omega_{p2}-\omega_{d2}$	$\omega_{p3}-\omega_{d2}$	$\omega_{p4}-\omega_{d2}$
3	$\omega_{p1}-\omega_{d3}$	$\omega_{p2}-\omega_{d3}$	$\omega_{p3}-\omega_{d3}$	$\omega_{p4}-\omega_{d3}$
4	$\omega_{p1}-\omega_{d4}$	$\omega_{p2}-\omega_{d4}$	$\omega_{p3}-\omega_{d4}$	$\omega_{p4}-\omega_{d4}$

[a]Assuming four data channels at ω_{di}, $i=1-4$; four SH clock phases at ω_{pj}, $j=1-4$. As long as the data channel spacing in the frequency domain equals the clock phase spacing, the diagonal elements are equal and can be selected by a bandpass filter.

and ω_c. $f(\Omega)$ is the bandpass filter function, and $\hat{A}_{\mathrm{os}}(\Omega)$ is the frequency-domain field envelope of the OTDM signal. $\hat{A}^2_{\mathrm{cl}}(\Omega)$ is the self-convolution of the external clock's frequency-domain envelope. $\hat{D}_{\mathrm{cg}}(\Omega)$ is the SHG transfer function of the clock-generation grating, and $\hat{D}_{\mathrm{sg}}(\Omega)$ is the sum of the DFG transfer functions of the four sampling gratings:

$$\hat{D}_{\mathrm{sg}}(\Omega)=\sum_{m=-1}^{2}\hat{D}_{\mathrm{DFG}}(\Omega+m\Delta\omega_d)e^{-j(\Omega+m\Delta\omega_d)\delta\nu mL_u}, \tag{2}$$

where $\Delta\omega_d$ is the frequency-domain data channel spacing, and we have assumed that the transfer functions of the sampling gratings are identical except for a shift of the center wavelength. The phase term comes from the shifted positions of the four sampling gratings. After the Fourier transform, the different phases translate into different times. $\hat{A}^2_{\mathrm{cl}}(\Omega)$, $\hat{D}_{\mathrm{cg}}(\Omega)$, and $\hat{D}_{\mathrm{DFG}}(\Omega)$ are explicitly defined in Ref. [7].

To generate four equal-amplitude SH clock phases from a first-harmonic (FH) pump with limited bandwidth, the clock generation grating was designed to have a transfer function with two outer spectral peaks larger than the inner ones, and the peak positions of $\hat{D}_{\mathrm{sg}}(\Omega)$ match those of $\hat{D}_{\mathrm{cg}}(\Omega)$ [Fig. 2(a)]. The spectrum resulting from the mixing of this SH clock and one data channel is shown in Fig. 2(b). After the bandpass filter, only one lobe is selected, and the contributions from the tails of $\hat{D}_{\mathrm{DFG}}(\Omega+m\Delta\omega_d)$ $(m\neq 0)$ become cross talk in the corresponding time slots [Fig. 2(c)].

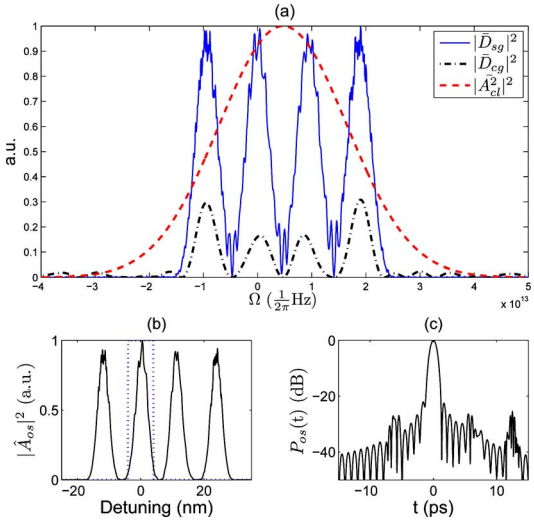

Fig. 2. (Color online) Calculated transfer functions, signal spectrum, and signal pulse shape.

We define the MUX efficiency as the ratio of signal to data pulse energy normalized to the square of the average clock power $\bar{P}_{\mathrm{cl}}$,

$$\eta_{\mathrm{MUX}}\equiv\frac{U_{\mathrm{os}}}{U_d\bar{P}^2_{\mathrm{cl}}}, \tag{3}$$

and quantify the cross talk as

$$X=\frac{\int_{T/2}^{3T/2}P_{\mathrm{os}}(t)\mathrm{d}t}{\int_{-T/2}^{T/2}P_{\mathrm{os}}(t)\mathrm{d}t}, \tag{4}$$

where T is the duration of one bit in the OTDM system and $P_{\mathrm{os}}(t)\propto|\int_{-\infty}^{\infty}\hat{A}_{\mathrm{os}}(\Omega)e^{i\Omega t}\mathrm{d}\Omega|^2$ is the time-domain power envelope of a signal pulse centered at $t=0$, obtained from the Fourier transform of $\hat{A}_{\mathrm{os}}$.

To demonstrate the MUX design, we fabricated the device using reverse proton-exchange (RPE) PPLN waveguides. Between the clock-generation grating and first sampling grating, there are two wavelength-selective directional couplers. Each coupler is 1.5 mm long, consisting of two parallel 6.5 μm wide waveguides separated by 2 μm. The first coupler serves to filter out the external FH clock; the second one couples data into the MUX. Given the constraint $L_u=17.36$ mm, the required length of the device exceeds the linear space available on a 3 in. diameter wafer. Integrating a 180° bend allowed us to double the available length. With a 2.39 μm initial proton-exchange depth, the minimum bend radius with negligible bending loss is 2 mm. The clock and data input and signal output ports are spaced by 250 μm to align with three optical fibers of a V-groove array. The clock-generation grating has two phase modulation periods and spans a total length of 4.47 mm. The average QPM period is 14.80 μm. It is designed for a data channel spacing of 11.5 nm. The peak ratios are designed to be 1.8:1:1:1.8 to compensate for the 25 nm FWHM of the external clock. The local nonlinear coupling of the 5.18 mm long sampling gratings is apodized according to $\kappa(z)\propto\cos^2(\pi z/L_{\mathrm{sg}})$ (grating center $z=0$) by the deleted-reversal technique [6]. The grating periods are 14.56, 14.68, 14.80, and 14.92 μm to match the wavelengths of the four-phase clock.

As no 40 GHz clock was available for this work, the MUX was tested with 150 fs 82 MHz C-band pulses from a Ti:sapphire-laser-pumped optical parametric oscillator (Spectra-Physics OPAL). The PPLN chip was held at 100 °C to protect it from photorefractive damage. The measured transfer function of the sampling gratings and the spectrum of the SH clock are shown in Fig. 3. The data confirm that the SH clock

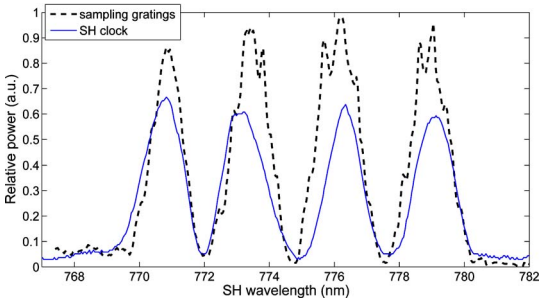

Fig. 3. (Color online) Spectral characterizations. Solid, spectrum of the SH clock; dashed, transfer function of the sampling gratings.

wavelengths matched the sampling gratings' pump acceptance bands and show that the four clock phases had approximately equal energy. One should not be surprised to see the fringes on the tuning curve peaks of sampling gratings. The SH waves generated in adjacent gratings were coherent, and they interfered. A −30 dB power contribution from an adjacent grating can account for ±7% power fluctuation at the peaks. This fluctuation is also seen in the theoretical curve in Fig. 2(a).

To test the integrated operation of the MUX, an amplified continuous wave (CW) laser was tuned to 1532.2, 1543.2, 1554.2, and 1565.2 nm to simulate the four data channels. The bandpass filter at the output had an 8 nm passband centered at 1549.8 nm. We resolved the time-domain envelope of the signal by cross correlating it with a fraction of the 150 fs OPO output (reference light) in an aperiodically poled lithium niobate [7] waveguide through sum frequency generation [8]. The CW laser was chopped at 1.5 kHz, and a lock-in amplifier distinguished the sum frequency generation from the spurious SH of reference. A piezo-actuated mirror provided 2π phase change to the reference beam at 10 kHz to average out any interference between the reference and the residual external clock from the MUX. Measured $P_{os}(t)$ values from all four channels are shown in Fig. 4. The small peaks to the left in all plots were the residual clock pulses. With 1 mW of average clock power and 60 mW of data power coupled into the MUX, the OTDM signal power was 9–14 μW for each channel. If the clock was scaled to 40 GHz at the same pulse energy, the corresponding efficiency would be 35%–50% W^{-2}. The low average signal power due to the low clock repetition rate, roughly 1/500 that of a real system, created some experimental difficulties. However, with the highly efficient aperiodically poled lithium niobate cross correlator, we were able to achieve a signal-to-noise ratio exceeding 20 dB. The electronic noise of the lock-in amplifier and $1/f$ noise of the reference light each accounted for half of the remaining noise floor. Short of a system test, the time-resolved measurements revealed the important figures of merit of the MUX. The measured (theoretical) signal pulse width (FWHM), time slot, data channel spacing, cross talk, and efficiency are 1.5 (1.7) ps, 6.2 (6.25) ps, 11 (11.5) nm, <−20 (−27) dB, and 35%–50% (68%) W^{-2}.

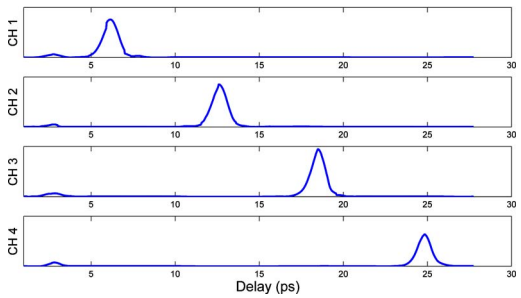

Fig. 4. (Color online) Measured OTDM signals from four data channels.

In summary, we have successfully designed a monolithic PPLN-based OTDM MUX and characterized its operation by using ultrafast-optical techniques. Its performance agreed well with theory. The proof-of-principle device had a slightly higher efficiency than a design previously demonstrated in Ref. [3]. With an optimized design, the data channel spacing can be reduced and efficiency doubled by using longer clock generation and sampling gratings.

In a future device, the residual clock pulse could be eliminated on chip by cascading multiple directional couplers. The loss of the deep exchange waveguides is approximately 0.4 dB/cm, compared with 0.1 dB/cm for conventional RPE waveguides. Ideally, the MUX would be fabricated on a 4 in. diameter wafer so that the tight U-turn bend would not be necessary and conventional RPE waveguides could be used.

We thank Crystal Technology for a generous donation of lithium niobate wafers. This research was supported by Air Force Office of Scientific Research grant FA9550-05-1-0180.

References

1. S. Kawanishi, IEEE J. Quantum Electron. **34**, 2064 (1998).
2. T. Ohara, H. Takara, I. Shake, K. Mori, S. Kawanishi, S. Mino, T. Yamada, M. Ishii, T. Kitoh, T. Kitagawa, K. Parameswaran, and M. Fejer, IEEE Photon. Technol. Lett. **15**, 302 (2003).
3. T. Ohara, H. Takara, I. Shake, K. Mori, K. Sato, S. Kawanishi, S. Mino, T. Yamada, M. Ishii, I. Ogawa, T. Kitoh, K. Magari, M. Okamoto, R. Roussev, J. Kurz, K. Parameswaran, and M. Fejer, IEEE Photon. Technol. Lett. **16**, 650 (2004).
4. M. Asobe, O. Tadanaga, H. Miyazawa, Y. Nishida, and H. Suzuki, Opt. Lett. **28**, 558 (2003).
5. J. Huang, J. Kurz, C. Langrock, A. Schober, and M. Fejer, Opt. Lett. **29**, 2482 (2004).
6. J. Huang, X. Xie, C. Langrock, R. Roussev, D. Hum, and M. Fejer, Opt. Lett. **31**, 604 (2006).
7. G. Imeshev, M. Arbore, M. Fejer, A. Galvanauskas, M. Fermann, and D. Harter, J. Opt. Soc. Am. B **17**, 304 (2000).
8. S. Yang, A. Weiner, K. Parameswaran, and M. Fejer, Opt. Lett. **29**, 2070 (2004).